Antarctic sea ice control on ocean circulation in present and glacial climates

Raffaele Ferrari[a,1], Malte F. Jansen[b], Jess F. Adkins[c], Andrea Burke[c], Andrew L. Stewart[c], and Andrew F. Thompson[c]

[a]Department of Earth, Atmospheric and Planetary Sciences, Massachusetts Institute of Technology, Cambridge, MA 02139; [b]Atmospheric and Oceanic Sciences Program, Geophysical Fluid Dynamics Laboratory, Princeton, NJ 08544; and [c]Division of Geological and Planetary Sciences, California Institute of Technology, Pasadena, CA 91125

Edited* by Edward A. Boyle, Massachusetts Institute of Technology, Cambridge, MA, and approved April 16, 2014 (received for review December 31, 2013)

In the modern climate, the ocean below 2 km is mainly filled by waters sinking into the abyss around Antarctica and in the North Atlantic. Paleoproxies indicate that waters of North Atlantic origin were instead absent below 2 km at the Last Glacial Maximum, resulting in an expansion of the volume occupied by Antarctic origin waters. In this study we show that this rearrangement of deep water masses is dynamically linked to the expansion of summer sea ice around Antarctica. A simple theory further suggests that these deep waters only came to the surface under sea ice, which insulated them from atmospheric forcing, and were weakly mixed with overlying waters, thus being able to store carbon for long times. This unappreciated link between the expansion of sea ice and the appearance of a voluminous and insulated water mass may help quantify the ocean's role in regulating atmospheric carbon dioxide on glacial–interglacial timescales. Previous studies pointed to many independent changes in ocean physics to account for the observed swings in atmospheric carbon dioxide. Here it is shown that many of these changes are dynamically linked and therefore must co-occur.

carbon cycle | ice age | ocean circulation | paleoceanography | Southern Ocean

The Last Glacial Maximum (LGM) spanning the period between about 25,000 and 20,000 y ago was characterized by global atmospheric temperatures 3–6° colder than today (1), atmospheric carbon dioxide (CO_2) concentrations 80–90 ppm lower than preindustrial values (2), and extended ice sheets and sea ice (3, 4). Geochemical tracers suggest that the ocean volume filled by waters of Antarctic origin was nearly quadrupled at the LGM (5). In this study we apply recent understanding of deep ocean dynamics to explain the connection between the observed changes in the atmosphere, the cryosphere, and the deep ocean water masses. This connection provides a robust framework to quantify the drop in atmospheric CO_2 concentrations, a critical gap in our understanding of glacial climates.

Much attention has been paid to the inferred changes in the deep ocean at the LGM, because they are believed to have played a key role in reducing atmospheric CO_2 concentrations (6–8). The deep ocean contains 90% of the combined oceanic, atmospheric, and terrestrial carbon, and a rearrangement of deep water masses could have a large impact on the atmospheric carbon budget. Fig. 1 shows the distributions of $\delta^{13}C$ of benthic foraminifera in the modern and glacial climates along a north–south section from the western Atlantic (5). In the modern section one can see the high $\delta^{13}C$ tongue of Arctic origin flowing over a low $\delta^{13}C$ tongue of Antarctic origin below 4 km. At the LGM, the Antarctic source water appears to fill the whole ocean volume below 2 km squeezing a much reduced component of Arctic source waters above 2 km.

The expansion of Antarctic-origin abyssal waters, richer in nutrients and metabolic carbon than the deep Arctic-origin waters it replaced, is believed to have reduced atmospheric CO_2 by 10–20 ppm (9). Concomitant changes in the ocean circulation, stratification, biological nutrient uptake, and carbonate compensation have been invoked to account for the full 80–90 ppm drawdown (10). The physical feedbacks that have been identified are (*i*) a change in the ocean circulation that isolates abyssal waters from the surface, possibly associated with an equatorward shift of the Southern Hemisphere westerlies (11–13), (*ii*) an increase in abyssal stratification acting as a lid to deep carbon (14), (*iii*) an expansion of sea ice that reduced the CO_2 outgassing over the Southern Ocean (15), and (*iv*) a reduction in the mixing between waters of Antarctic and Arctic origin, which is a major leak of abyssal carbon in the modern climate (16). Current understanding is that some combination of all of these feedbacks, together with a reorganization of the biological and carbonate pumps, is required to explain the observed glacial drop in atmospheric CO_2 (17). Here we apply theories of the deep ocean circulation to illustrate that there is a direct dynamical link between the drop in temperature, the expansion of sea ice around Antarctica, the rearrangement of the ocean deep water masses, and the change in circulation at the LGM. Hence these are not independent feedbacks, rather they are expected to co-occur in each glacial cycle and may explain why the atmospheric CO_2 concentrations dropped by the same amount for at least the last four glacial cycles.

Modern Deep Ocean Stratification and Circulation

Munk (18) first argued that the dense ocean waters that sink through convection into the abyss at high latitudes return back to the surface as they are mixed by turbulence with lighter overlying waters. In this conceptual model, high-latitude convection sets the rate of the overturning circulation, and mixing determines the deep ocean stratification through a balance between upwelling of dense waters and downward diffusion of light waters. This view ignored the pivotal role of the Southern Ocean (SO) in controlling both the stratification and the overturning of deep water masses (19–21). In this section we review key elements of the new paradigm that has emerged over the last twenty years. In the next section we discuss its implications for interpreting the changes observed in the ocean at the LGM.

Significance

The ocean's role in regulating atmospheric carbon dioxide on glacial–interglacial timescales remains an unresolved issue in paleoclimatology. Many apparently independent changes in ocean physics, chemistry, and biology need to be invoked to explain the full signal. Recent understanding of the deep ocean circulation and stratification is used to demonstrate that the major changes invoked in ocean physics are dynamically linked. In particular, the expansion of permanent sea ice in the Southern Hemisphere results in a volume increase of Antarctic-origin abyssal waters and a reduction in mixing between abyssal waters of Arctic and Antarctic origin.

Author contributions: R.F. designed research; R.F., M.F.J., J.A., A.B., A.L.S., and A.F.T. performed research; R.F. and M.F.J. analyzed data; and R.F. wrote the paper.

The authors declare no conflict of interest.

*This Direct Submission article had a prearranged editor.

Freely available online through the PNAS open access option.

[1]To whom correspondence should be addressed. E-mail: rferrari@mit.edu.

This article contains supporting information online at www.pnas.org/lookup/suppl/doi:10.1073/pnas.1323922111/-/DCSupplemental.

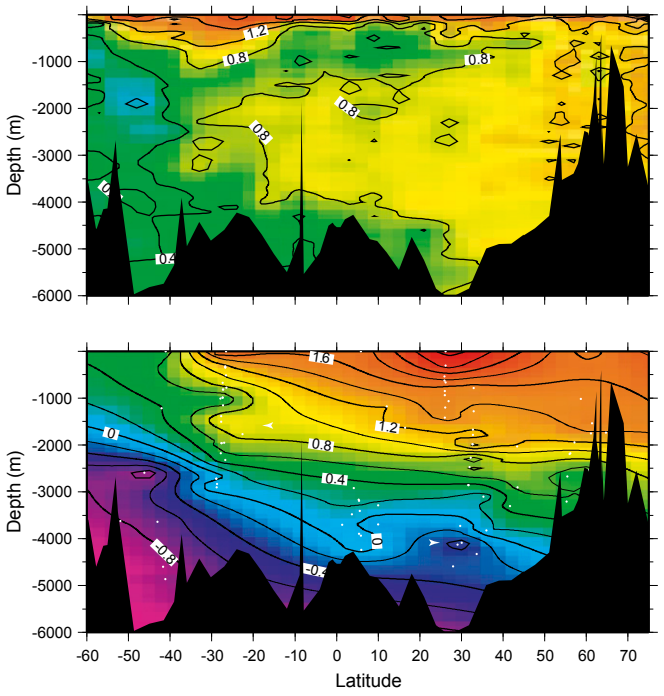

Fig. 1. Contour maps of $\delta^{13}C$ for a section in the Western Atlantic (5) based on water samples for the modern climate (*Upper*) and benthic foraminiferal stable isotope data using a variety of *Cibicidoides spp*. for the LGM (*Lower*). The glacial reconstruction documents the shoaling of North Atlantic Deep Water to about 1,500 m, and the expansion and northward penetration of Southern Ocean Deep Water/Antarctic Bottom Water.

Fig. 2 shows the zonally averaged distribution of density in the global ocean based on the World Ocean Circulation Experiment (WOCE) hydrographic atlas (23). Herein by density we mean neutral density, that is the density corrected to eliminate dynamically irrelevant compressive effects that increase the water density at depth (22). Values are reported in kg m^{-3} subtracting 1000 kg m^{-3}, so a neutral density of 28 kg m^{-3} is actually 1,028 kg m^{-3}. Density surfaces, herein isopycnals, are approximately flat between 50°S and 50°N, except for the two bowls of light waters in the upper 500 m, on the two sides of the equator, which are the result of wind-driven circulations (24). South of 50°S, in the latitude band of the SO, and north of 50°N in the North Atlantic, the isopycnals develop a substantial slope. Keeping in mind that the large-scale oceanographic flows are directed primarily along isopycnals, it follows that the SO and the North Atlantic are the primary conduits through which the deep ocean exchanges properties with the atmosphere.

Ocean Stratification. The slope of isopycnals in the SO is set by a balance between winds and instabilities of the major currents (25). The Southern Hemisphere westerlies drive a clockwise overturning circulation with water moving equatorward at the surface. This flow acts to steepen isopycnals, but instabilities develop that generate a counterclockwise overturning circulation that slumps isopycnals back to the horizontal. An equilibrium is achieved between the wind and instability driven overturning circulations when the isopycnal slope s is approximately equal to:

$$s \simeq \frac{\tau}{\rho_0 f K}, \qquad [1]$$

where τ is the local surface wind stress, ρ_0 is a reference surface density (seawater is weakly compressible and the density is everywhere within a few percent of 1,027 kg m^{-3}), f is the Coriolis frequency equal to twice the Earth's rotation rate multiplied by the sine of the latitude, and K is an eddy diffusivity that quantifies the efficiency of instabilities at slumping isopycnals. This formula holds in a zonally averaged sense or, more precisely, for an average along the path of the Antarctic Circumpolar Current (ACC) that flows around the whole globe in the SO.

To illustrate the power of the scaling law **1**, we plot the prediction for the slope of isopycnal 27.9 kg m^{-3}, which outcrops in the surface winter mixed layer at 65°S, for a characteristic wind stress of 0.1 N m^{-2} and eddy diffusivity $K = 1{,}000$ m^2 s^{-1} (25). The black dashed line in Fig. 2 shows that with these values, the scaling **1** correctly predicts the slope of isopycnals shallower than 3,000 m; i.e., above major topographic ridges and seamounts, which modify somewhat the slope of deeper isopycnals. In the upper few hundred meters, the isopycnals become flat at latitudes where winter ice melts and creates a shallow layer of fresh water. This is a transient summer phenomenon. Our scaling applies to isopycnals below this layer.

Given the surface distribution of density, the scaling for the slope determines the zonally averaged distribution of density below the shallow wind-driven bowls. The argument is purely geometrical, and it is illustrated by the dashed black line in Fig. 2. The isopycnals slope downward from the latitude where they intersect the surface (more appropriately the base of the surface mixed layer) to approximately 45° S, the northernmost latitude reached by the ACC where Eq. **1** holds. North of 45° S, the isopycnals are essentially flat, because the presence of lateral boundaries does not permit strong zonal flows, which would result in tilted isopycnals. Density surfaces lighter than 28 kg m^{-3} come to the surface also at high latitudes in the North Atlantic with a very steep slope in response to upright convection driven by strong cooling.

These simple scaling arguments provide sufficient information to rationalize the most conspicuous changes observed in the ocean at the LGM. However, they are not a self-contained theory of the ocean stratification, because they require knowledge of the surface density distribution in the SO and the maximum latitude reached by the ACC. Also they ignore important departures from zonality. The ACC extends farther north in the Pacific sector than in the Atlantic and, as a result, the same isopycnal tends to be nearly 500 m deeper in the Pacific Ocean than in the Atlantic Ocean.

Southern Ocean Overturning Circulation. The density distribution implied by the scaling **1** and shown in Fig. 2 can be used to diagnose the zonally averaged overturning circulation in the SO. We begin from the meridional flow at the ocean surface. Fig. 3 shows the annual averaged air–sea buoyancy flux based on an ocean state estimate that combines available observations (26). Buoyancy is defined as $b = -g(\rho - \rho_0)/\rho_0$, i.e. the departure of density ρ from a reference value $\rho_0 = 1{,}027$ kg m^{-3} and multiplied by the gravitational acceleration. The buoyancy flux is the flux of

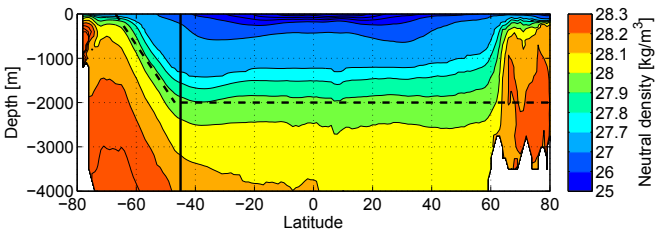

Fig. 2. Zonally averaged neutral density surfaces based on the WOCE hydrographic atlas (23). The vertical line marks the 45°S latitude, the northernmost latitude reached by the Antarctic Circumpolar Current. The dashed line is the theoretical prediction based on Eq. **1** for the shape of the density surface 27.9 kg m^{-3} outcropping at the summer sea ice edge in the Southern Hemisphere.

density across the air–sea interface generated by heating/cooling and evaporation/precipitation, except for a change in sign. A positive buoyancy flux means that the ocean is becoming lighter because of warming, precipitation, or ice melting. A negative buoyancy flux represents cooling, evaporation, or brine rejection by ice freezing. The buoyancy flux in Fig. 3 is negative around coastal Antarctica where the relatively warm subsurface waters that upwell in the SO are cooled to the freezing point and become saltier through brine rejection as new ice is formed. The buoyancy flux is positive farther north where sea ice is only seasonal and the ocean is warmed in summer by the atmosphere and freshened by ice melting. The sign of the yearly average buoyancy flux constrains the direction of the zonally and time-averaged surface meridional flow. The density of surface waters increases toward the poles and hence waters must become denser (lighter) to move poleward (equatorward). A surface-density gain (loss) is achieved when waters are exposed to a negative (positive) buoyancy flux. Thus, the surface meridional flow in a steady state must be directed poleward where the buoyancy flux is negative and equatorward where the buoyancy flux is positive. This is a key insight for the rest of our argument.

The meridional surface flow, together with the realization that water masses flow along isopycnals below the surface (25), can be used to diagnose the two branches of the SO overturning. Today the isopycnal 27.9 kg m^{-3}, marked as a black dashed line in Fig. 2, intersects the surface approximately where the air–sea buoyancy flux changes sign. An upward isopycnal flow must develop to feed the divergent surface flow: surface waters south of the isopycnal experience a negative buoyancy flux and thus flow poleward, and surface waters north of the isopycnal flow equatorward in response to the positive buoyancy flux. The resulting circulation pattern is composed of two overturning branches. The lower branch comes to the surface parallel, but below, the dividing isopycnal; flows poleward along the surface; and then sinks into the abyss around Antarctica (along the Antarctic continental margin, brine rejection makes the waters so dense that they plunge into the abyss along boundary overflows.) The upper branch, instead, comes to the surface above the dividing isopycnal, flows equatorward at the surface and then sinks along isopycnals as intermediate waters, below the shallow wind-driven bowls. The two branches of the overturning circulations are sketched in Fig. 4 and are identified in ocean observations (27–29). This diagnostic argument suggests that the patterns of the overturning circulation can be reconstructed from knowledge of the line where the air–sea buoyancy flux changes sign in the SO.

This argument is, however, useful only if we find a paleoproxy for the surface buoyancy flux. The negative buoyancy flux around Antarctica arises under permanent sea ice, where the heat fluxes are weak and salinity fluxes are strong due to brine rejection. The solid white line in Fig. 3 confirms that the transition between negative and positive buoyancy flux closely coincides with the extent of the quasi-permanent sea ice line, here defined as the ocean area covered by sea ice 70% of the year. This suggests that the area of negative buoyancy flux scales with the extent of the quasi-permanent sea ice. Hence we surmise that the separation between the upper and lower overturning branches shifts with the expansion and contraction of sea ice in different climates. This is the key hypothesis pursued below. However, first, we must describe how the two SO overturning branches complete their journey through the three ocean basins north of the SO.

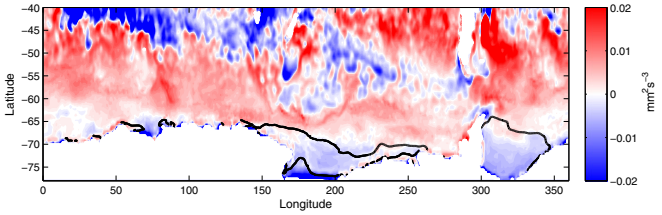

Fig. 3. Annual mean buoyancy flux from a state estimate that combines 3 y of available observations with an ocean model (26). The black line denotes the 70% quantiles of annual mean sea ice concentration, essentially the area of the ocean covered by ice 70% of the time. The change in sign of the buoyancy flux just north of the Antarctic continent is roughly colocated with the 70% quantile of sea ice coverage.

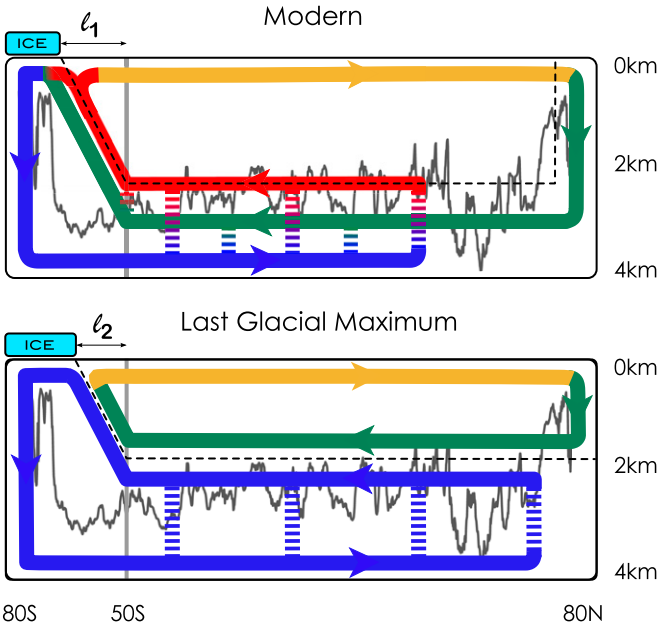

Fig. 4. (*Upper*) Schematic of the overturning circulation for the modern climate. The ribbons represent a zonally averaged view of the circulation of the major water masses; blue is AABW, green is NADW, red are IDW and PDW, and orange are Antarctic Intermediate Waters. The dashed vertical lines represent mixing-driven upwelling of AABW into NADW and IDW/PDW respectively. There is also some mixing between NADW and IDW/PDW in the Southern Ocean. The dashed black line represents the isopycnal that separates the upper and lower overturning branches present in the Southern Ocean. ℓ_1 is the distance between the northernmost latitude reached by the ACC, indicated by a solid gray line, and the quasi-permanent sea ice line. The ragged gray line is the crest of the main bathymetric features of the Pacific and Indian ocean basins: mixing is enhanced below this line. (*Lower*) Schematic of the overturning circulation for the LGM. The extent of the quasi-permanent sea ice line has shifted equatorward compared with modern climate ($\ell_2 < \ell_1$). Mixing-driven upwelling of abyssal waters is confined below 2 km and it cannot lift waters high enough to upwell north of the ice line. As a result the abyssal overturning circulation closes on itself, leaving above a small overturning cell of North Atlantic waters.

Atlantic, Indian, and Pacific Ocean Overturning Circulations. Talley (30) gives an excellent review of our current understanding of the pathways of the overturning circulation in the global ocean based on estimates of the heat, freshwater, and nutrient transports. The schematic in Fig. 4 highlights some key results relevant for this study, at the expense of ignoring all of the complexities of the large-scale 3D circulation.

The overturning circulation is dominated by the intertwined pathways of abyssal waters, deep waters, and intermediate waters illustrated as ribbons of different colors in Fig.4. We begin our description of the overturning from the formation of deep waters through wintertime convection in the North Atlantic. The North Atlantic Deep Water (NADW) flows southward primarily along deep western boundary currents all of the way to the SO, where it is brought to the surface along isopycnals by the Southern

Hemisphere westerlies (green ribbon). The core of NADW has densities of 28 kg m^{-3} and thus upwells in the SO south of the isopycnal 27.9 kg m^{-3}, where the buoyancy flux is negative. It then flows southward toward Antarctica, where it is subject to brine rejection and sinks back into the abyss. These dense waters flow northward as Antarctic Bottom Water (AABW) at the bottom of the Atlantic, Indian, and Pacific Oceans (blue ribbon). In all three oceans, AABW upwells into the local deep water; that is, into NADW in the Atlantic (green ribbon), Indian Deep Water in the Indian (IDW; red ribbon), and Pacific Deep Water in the Pacific (PDW; red ribbon). The transformation from abyssal to deep waters is driven by turbulent mixing, which diffuses waters across density surfaces (dashed vertical ribbons). Observations and theory, reviewed in the *Supporting Information*, show that mixing is most vigorous below 2 km, where internal waves radiated from rough topography break and mix (31, 32). AABW therefore diffuses up to a depth of 2 km in the Indian and Pacific Oceans before returning to the SO along isopycnals. In the North Atlantic, AABW does not diffuse as far up because it has less time to mix into the faster flowing NADW. The IDW and PDW have core densities around 27.9 kg m^{-3} and outcrop in the SO farther to the north than the denser NADW. The upwelled IDW/PDW feed both branches of the overturning in the SO: a fraction of the waters upwell north of the buoyancy flux line and flow across the ACC to join the upper branch, the rest is recycled back through the lower branch along with NADW. The fraction of IDW/PDW that joins the upper branch is a major source of the intermediate waters that flows northward to the NADW formation region (orange ribbon), again connecting the upper and lower branches.

An important aspect of the circulation is that turbulent mixing sets the depth to which AABW upwells in the Indian and Pacific Oceans. The 27.9 kg m^{-3} isopycnal that separates the upper and lower SO overturning branches sits close to 2 km in the Indian and Pacific Oceans, and it is a bit shallower in the Atlantic Ocean for the reasons pointed out above. (We follow ref. 30 in choosing 27.9 kg m^{-3} as the isopycnal that separates the SO overturning branches. This is the same density that separates the two branches of the overturning in the Southern Ocean in ref. 28.) Abyssal mixing is enhanced below 2 km, the characteristic depth of midocean ridges. In the modern climate, this depth is sufficiently shallow and the summer sea ice line sufficiently far south that a substantial fraction of IDW and PDW upwell north of the zero buoyancy flux line and thus join the upper branch. The modern overturning circulation is more akin to a figure eight loop than two separate loops.

Glacial Deep Ocean Stratification and Circulation

Reconstructions based on a combination of available proxy and numerical models suggest that global surface temperatures at the peak of the last glacial period were between 3° and 6° colder than in preindustrial times (1), with even more pronounced cooling south of 45°S (4). Such a cooling is expected to cause the latitude range of above-freezing temperatures to contract. Summer sea ice tracks the −2 °C isoline of surface temperature (the temperature at which sea water freezes), and thus the surface cooling is expected to have resulted in an expansion of the area covered by sea ice. Diatom and radiolarian assemblages from sediment cores confirm that the summer sea ice expanded at the LGM, but the data are too sparse to determine the overall areal expansion (3).

Numerical simulations suggest that the sea ice coverage expanded during glacial climates, following the equatorward shift of the −2 °C summer air temperature isoline. In Fig. 5 we show output from two National Center for Atmospheric Research Community Climate System Model version 3 (CCSM3) model simulations run for modern and LGM climates (33). The solid black lines, which mark the quasi-permanent sea ice line, shifted in excess of 5° latitude at the LGM, together with the area where the air–sea buoyancy flux is negative. Such an expansion is not inconsistent with the diatom and radiolarian reconstructions. (In the state estimate for the modern climate, the zero buoyancy flux lines follows the ocean area covered by ice 70% of the time, while in the simulations it follows more closely the ocean area covered by ice 80% of the time. This slight difference may reflect deficiencies in the sea ice model or the limited temporal coverage of the observations (3 y). Regardless, our argument is that the buoyancy flux is negative where the ocean is covered by ice most of the year and it does not matter whether most means 70% or 80%.)

Following the scaling argument given in the previous section, we can reconstruct the impact of a shift in the quasi-permanent sea ice line, and the associated zero buoyancy flux line, on the ocean stratification and overturning. In the SO, the isopycnal that separates the upper and lower branches of the overturning has a slope s given by Eq. **1** and outcrops at the zero buoyancy flux line. The depth of this isopycnal, once it reaches the closed oceans basins and becomes flat, is therefore given by:

$$D \simeq \ell \times s, \qquad [2]$$

where ℓ is the distance between the quasi-permanent sea ice line and the northern extent of the ACC (see the schematic in Fig. 4). In the modern climate $s \simeq 10^{-3}$, and the distance between the quasi-permanent sea ice line (65°S) and the northern boundary of the ACC (45°S) is close to 20° latitude or close to 2,200 km. This gives a depth $D \simeq 2.2$ km, which is close to the depth of the isopycnal 27.9 kg m^{-3} in the Pacific and somewhat deeper than the same isopycnal in the Atlantic.

A 5° latitude shift of the quasi-permanent sea ice line is equal to a $\delta\ell$ decrease of close to 500 km. For a constant isopycnal slope s this results into a 500-m shoaling ($s \times \delta\ell$) of the isopycnal separating the lower and upper branches of the SO overturning. As the isopycnal shoals above 2 km in the ocean basins, turbulent mixing is no longer able to drive substantial upwelling of AABW across the isopycnal. Strong turbulent mixing is confined below 2 km both in the modern climate and the LGM, because it is generated in proximity of seamounts and midocean ridges, which are mostly confined below 2 km. As a consequence, the deep waters return to the SO below the isopycnal outcropping at the

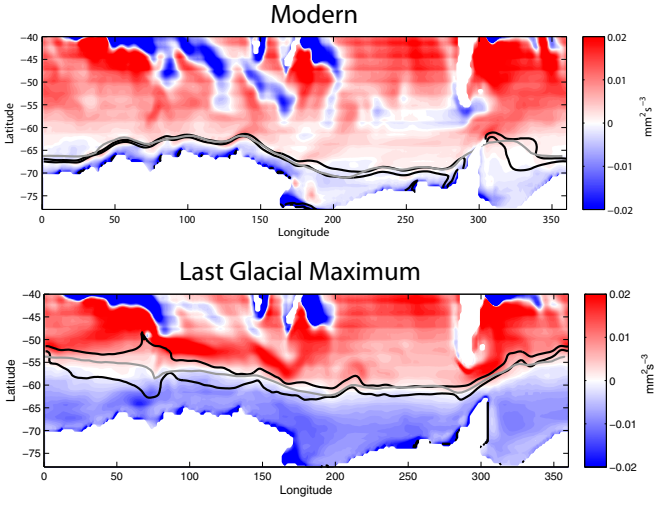

Fig. 5. The surface buoyancy flux from two CCSM3 simulations run for modern and LGM climates (33). The flux is in color with blue representing negative fluxes. The black lines are the 70% and 80% quantiles of annual mean sea ice concentration. The gray line is the position of the −2 °C air temperature isoline at 2 m in summer. The area of negative buoyancy flux, the −2 °C isoline and the extent of quasi-permanent sea ice shift poleward in excess of 5° latitude at the LGM.

sea ice line, upwell under quasi-permanent ice, where the buoyancy flux is negative, and move toward Antarctica to be transformed back into AABW (blue ribbon in Fig. 4*B*). In response the NADW shoals above the expanded abyssal cell to outcrop where the buoyancy flux is positive, and return north as intermediate waters completing a closed loop (green and yellow ribbons in Fig. 4, *Lower*.) Any NADW sinking below 2 km would outcrop under sea ice and be transformed into denser AABW, never to come back to the North Atlantic. The transformation of waters from the upper to the lower cell would continue during a transient, until the NADW neutral buoyancy level shoaled above 2 km. The inescapable conclusion is that a 5° latitude expansion of quasi-permanent sea ice would result in two separate overturning cells on top of each other. This is the paradigm that is sometimes erroneously sketched for the modern climate. A more detailed explanation of how the ocean overturning transitions from a figure eight loop to two separate loops is given in the *Supporting Information*.

In summary, the 5° latitude expansion of summer sea ice at the LGM was accompanied by the splitting of the modern figure eight overturning circulation in two separate overturning cells as illustrated in Fig. 4. As a result waters of Antarctic origin filled all ocean basins up to 2 km depth, instead of the present 4 km depth. These changes are consistent with the rearrangement of water masses documented in paleorecords. The $\delta^{13}C$ map in Fig. 1 shows that the LGM ocean was filled with waters of Antarctic origin below 2 km. Other deep nutrient ocean tracers confirm this inference (34–36). Profiles of $\delta^{18}O$ show that the temperature and salinities (the two variables that affect $\delta^{18}O$) of the deep Atlantic below 2 km reflect their Southern Ocean origin with no signature of a saltier and warmer NADW (37). Atlantic and Pacific deep nutrient distributions were more similar at the LGM than today suggesting a common origin (38). The similarity in nutrient distributions above 2 km in the LGM Atlantic and Indian Oceans is further evidence of a shallow overturning circulation separate from abyssal water masses (39).

Estimates of radiocarbon water mass "ages" also support our simple theory. In the present day Indian and Pacific Oceans, there is a middepth maximum in water ages because AABW is younger than the returning IDW/PDW. In the Atlantic Ocean, there is no age maximum, because the fast flowing NADW is younger than the slow AABW. Our inference that AABW returned south as deep waters below North Atlantic source waters at the LGM (blue ribbon in Fig. 4, *Lower*) points to the appearance of a middepth age maximum in the Atlantic as well. Radiocarbon deep ventilation ages confirm that middepth waters in the South Atlantic were 2,000–3,750 y old (40), sandwiched between much younger waters above (41) and below (42). Further work will need to quantitatively assess the comparison of our model with the radiocarbon profiles.

Our argument so far ignored variations in isopycnal slope between present day and glacial climates. This is at odds with the recent literature on the role of changes in the strength and location of winds at the LGM (12, 13, 43), which in turn set the isopycnal slope. Eq. **2** can be used to estimate the relative importance of changes in sea ice line versus changes in wind stress on the stratification and overturning at the LGM. Changes in the depth of the interface between the upper and lower branches of the SO overturning, δD, scale as,

$$\frac{\delta D}{D} \simeq \frac{\delta s}{s} + \frac{\delta \ell}{\ell} \simeq \frac{\delta \tau}{\tau} - \frac{\delta K}{K} + \frac{\delta \ell}{\ell}, \qquad [3]$$

where we used Eq. **1** to relate the changes in slope to changes in SO wind stress, $\delta\tau$, and eddy diffusivity, δK. Paleoreconstructions and atmospheric models suggest that the strength of winds changed by less than 10% at the LGM either due to a few degrees poleward shift of the westerlies or a strengthening of the surface temperature gradient (44, 45). However changes in δK tend to strongly compensate any increase/decrease in the winds (46–48): instabilities release the wind energy input in the ocean, so K increases/decreases as the winds increase/decrease. The combined effect of changes in winds and eddy diffusivities would thus appear to imply a shoaling/deepening of the isopycnal separating the two branches of the SO overturning closer to 1% than 10%. This is to be contrasted with the 25% change that we estimated from the sea ice line shift ($\delta\ell/\ell = 500/2{,}000$).

Conclusions

Our analysis suggests that the observed expansion of deep waters of Antarctic origin at the LGM is dynamically linked to the expansion of quasi-permanent (summer) sea ice in the Southern Hemisphere. The argument is best explained through the schematic shown in Fig. 4. The overturning circulation in the Southern Ocean is dominated by two major branches: an abyssal branch with waters upwelling under summer sea ice and sinking into the abyss around Antarctica, and a deep branch with waters upwelling north of the summer sea ice line and flowing to the north. The isopycnal that intersects the surface at the summer sea ice line separates the two overturning branches along a surface of constant slope in the SO and along a flat surface in the ocean basins to the north (dashed lines in Figs. 2 and 4). In the modern climate, the summer sea ice edge is close to Antarctica and the isopycnal plunges below 2 km depth before reaching the ocean basins. There are many topographic features that reach this depth resulting in strong mixing that drives waters across the dividing isopycnal and connects the two branches of the overturning circulation in a single figure eight overturning cell. At the LGM, the summer sea ice line shifted northward by at least 500 km according to paleoreconstructions and numerical models. The density budget of the ocean demands that the isopycnal separating the two overturning branches of the circulation shifted together with the sea ice line, as shown in Fig. 4, *Lower*, and did not plunge as deep into the ocean basins (the slope of this surface changes little across different climates.) Once the isopycnal shoaled above 2 km, it did not intersect much topography and experienced little turbulent mixing so that the two overturning branches became two separate closed overturning cells stacked one on top of the other. The traditional view of two separate overturning cells, incorrectly used at times to describe the modern ocean, is only appropriate for the LGM climate.

Deep ocean tracer distributions are consistent with Antarctic origin waters filling all oceans below 2 km at the LGM and only below 4 km in the modern climate (Fig. 1). Our analysis suggests that this expansion tracks the appearance of a closed abyssal overturning cell coming to the surface only around Antarctica under sea ice. This voluminous water mass was likely very salty as it experienced strong brine rejection under the sea ice, consistent with porous fluid measurements (49); see the *Supporting Information*.

The dynamical model presented here provides solid underpinning for quantifying the role of ocean circulation on the glacial carbon budget. The ocean–atmosphere partitioning of carbon is set by a balance between biological carbon export from the surface ocean, the "biological pump," the return of carbon to the surface by the ocean's overturning circulation, the "physical pump" (6–8) and a whole-ocean carbon compensation response (50). Our work shows that the primary changes in the glacial physical pump consisted of three effects. The LGM waters filling all deep oceans below 2 km were at freezing temperature, thus increasing the seawater solubility of CO_2. The LGM deep waters leaked less carbon than today, because they did not experience much mixing with the overlying waters of North Atlantic origin (16), and they outcropped only under summer sea ice, possibly experiencing little surface outgassing of CO_2 (15). Finally the fourfold expansion of poorly ventilated waters at the LGM (the ocean waters below 2 km occupy 4 times the volume of waters below 4 km) increased the ocean storage capacity of carbon at depth (51). An assessment of the atmospheric CO_2 drawdown in

response to these physical changes would require a quantification of the associated changes in the biological pump and the carbon compensation (10). Our focus has rather been to identify what changes in the physical pump are dynamically linked and must have co-occurred at the LGM. This insight should help focus future studies of the glacial carbon cycle on physically realizable ocean states and allow a more effective exploration of the changes in biological productivity and carbon compensation.

It is important to emphasize that we proposed a diagnostic reconstruction that connects sea ice expansion, ocean overturning circulation, and deep water masses. This is different from proposing a prognostic theory for how the ocean transitioned from the modern to a glacial climate. The sea ice expansion could have been triggered by a temperature drop in the Northern or in the Southern Hemisphere. The power of our argument is to show that disparate observations of the LGM climate can be brought together into a unified framework through ocean dynamics. Future work will need to assess to what extent the zonally averaged approach introduced in this study captures the major features of the 3D ocean circulation at the LGM.

ACKNOWLEDGMENTS. L.P. Nadeau helped with figures. All authors acknowledge support from the National Science Foundation. R.F. acknowledges support from the Breene M. Kerr Chair.

1. Schneider von Deimling T, Ganopolski A, Held H, Rahmstorf S (2006) How cold was the last glacial maximum? *Geophys Res Lett* 33(14):L14709.
2. Monnin E, et al. (2001) Atmospheric CO2 concentrations over the last glacial termination. *Science* 291(5501):112–114.
3. Gersonde R, Crosta X, Abelmann A, Armand L (2005) Sea-surface temperature and sea ice distribution of the southern ocean at the EPILOG last glacial maximum—A circum-antarctic view based on siliceous microfossil records. *Quat Sci Rev* 24(7-9):869–896.
4. MARGO Project Members (2009) Constraints on the magnitude and patterns of ocean cooling at the last glacial maximum. *Nat Geosci* 2:127–132.
5. Curry WB, Oppo DW (2005) Glacial water mass geometry and the distribution of δ^{13} C of $\sum CO_2$ in the western Atlantic Ocean. *Paleoceanography* 20(1):PA1017.
6. Knox F, McElroy MB (1984) Changes in atmospheric co2: Influence of the marine biota at high latitude. *J Geophys Res Atmos* 89:4629–4637.
7. Sarmiento JL, Toggweiler JR (1984) A new model for the role of the oceans in determining atmospheric pCO2. *Nature* 308:621–624.
8. Siegenthaler U, Wenk T (1984) Rapid atmospheric co2 variations and ocean circulation. *Nature* 308:624–626.
9. Brovkin V, Ganopolski A, Archer D, Rahmstorf S (2007) Lowering of glacial atmospheric CO2 in response to changes in oceanic circulation and marine biogeochemistry. *Paleoceanography* 22:PA4202.
10. Hain MP, Sigman DM, Haug GH (2010) Antarctic stratification, North Atlantic Intermediate Water formation, and subantarctic nutrient drawdown during the last ice age: Diagnosis and synthesis in a geochemical box model. *Global Biogeochem Cycles* 24:47–55.
11. Sigman DM, Altabet MA, Francois R, McCorkle DC, Gaillard J-F (1999) The isotopic composition of diatom-bound nitrogen in southern ocean sediments. *Paleoceanography* 14(2):118–134.
12. Anderson RF, et al. (2009) Wind-driven upwelling in the Southern Ocean and the deglacial rise in atmospheric CO_2. *Science* 323(5920):1443–1448.
13. Toggweiler JR (2009) Climate change. Shifting westerlies. *Science* 323(5920):1434–1435.
14. de Boer AM, Sigman DM, Toggweiler JR, Russell JL (2007) Effect of global ocean temperature change on deep ocean ventilation. *Paleoceanography* 22(2):PA2210.
15. Stephens BB, Keeling RF (2000) The influence of Antarctic sea ice on glacial-interglacial CO_2 variations. *Nature* 404(6774):171–174.
16. Lund DC, Adkins JF, Ferrari R (2011) Abyssal Atlantic circulation during the Last Glacial Maximum: Constraining the ratio between transport and vertical mixing. *Paleoceanography* 26.
17. Sigman DM, Hain MP, Haug GH (2010) The polar ocean and glacial cycles in atmospheric $CO_{(2)}$ concentration. *Nature* 466(7302):47–55.
18. Munk WH (1966) Abyssal recipes. *Deep-Sea Res* 13:707–730.
19. Toggweiler JR, Samuels B (1998) On the ocean's large-scale circulation near the limit of no vertical mixing. *J Phys Oceanogr* 28:1832–1852.
20. Gnanadesikan A (1999) A simple predictive model for the structure of the oceanic pycnocline. *Science* 283(5410):2077–2079.
21. Nikurashin M, Vallis G (2011) A theory of deep stratification and overturning circulation in the ocean. *J Phys Oceanogr* 41:485–502.
22. Jackett DR, McDougall TJ (1997) A neutral density variable for the world's oceans. *J Phys Oceanogr* 27(9):237–263.
23. Deutsches Ozeanographisches Datenzentrum/Bundesamt Fur Seeschifffahrt Und Hydrographie/Germany(2006) *The World Ocean Circulation Experiment (WOCE) Global Hydrographic Climatology*. Available at http://rda.ucar.edu/datasets/ds285.4/. Accessed May 21, 2014.
24. Pedlosky J (1987) *Geophysical Fluid Dynamics* (Springer, New York).
25. Marshall J, Speer K (2012) Closure of the meridional overturning circulation through Southern Ocean upwelling. *Nat Geosci* 5:171–180.
26. Mazloff MR, Heimbach P, Wunsch C (2010) An eddy-permitting Southern Ocean state estimate. *J Phys Oceanogr* 40:880–899.
27. Ganachaud A, Wunsch C (2000) Improved estimates of global ocean circulation, heat transport and mixing from hydrographic data. *Nature* 408(6811):453–457.
28. Lumpkin R, Speer K (2007) Global ocean meridional overturning. *J Phys Oceanogr* 37: 2550–2562.
29. Talley LD, Reid JL, Robbins PE (2003) Data-based meridional overturning streamfunctions for the global ocean. *J Clim* 16:3213–3226.
30. Talley LD (2013) Closure of the global overturning circulation through the Indian, Pacific and Southern Oceans: Schematics and transports. *Oceanography* 26:80–97.
31. St. Laurent LC, Simmons HL, Jayne SR (2002) Estimating tidally driven mixing in the deep ocean. *Geophys Res Lett* 29:21-1–21-4.
32. Nikurashin M, Ferrari R (2013) Overturning circulation driven by breaking internal waves in the deep ocean. *Geophys Res Lett* 40:3133–3137.
33. Otto-Bliesner BL, et al. (2007) Last Glacial Maximum ocean thermohaline circulation: PMIP2 model intercomparisons and data constraints. *Geophys Res Lett* 34:L12706.
34. Boyle EA, Keigwin LD (1982) Deep circulation of the North Atlantic over the last 200,000 years: Geochemical evidence. *Science* 218(4574):784–787.
35. Curry WB, Lohmann GP (1982) Carbon isotopic changes in benthic foraminifera from the western South Atlantic: Reconstruction of glacial abyssal circulation patterns. *Quat Res* 18:218–235.
36. Duplessy JC, et al. (1988) Deepwater source variations during the last climatic cycle and their impact on the global deepwater circulation. *Paleoceanography* 3:343–360.
37. McCave IN, Carter L, Hall IR (2008) Glacial-interglacial changes in water mass structure and flow in the sw Pacific Ocean. *Quat Sci Rev* 27:1886–1908.
38. Boyle EA (1988) Cadmium: Chemical tracer of deepwater paleoceanography. *Paleoceanography* 3:471–489.
39. Boyle EA (1997) Characteristics of the deep ocean carbon system during the past 150,000 years: SigmaCO2 distributions, deep water flow patterns, and abrupt climate change.$\sum CO_2$. *Proc Natl Acad Sci USA* 94(16):8300–8307.
40. Skinner LC, Fallon S, Waelbroeck C, Michel E, Barker S (2010) Ventilation of the deep Southern Ocean and deglacial CO_2 rise. *Science* 328(5982):1147–1151.
41. Burke A, Robinson LF (2012) The Southern Ocean's role in carbon exchange during the last deglaciation. *Science* 335(6068):557–561.
42. Barker S, Knorr G, Vautravers MJ, Diaz P, Skinner L (2010) Extreme deepening of the Atlantic circulation during deglaciation. *Nat Geosci* 291:567–571.
43. Toggweiler JR, Russell J, Carson SR (2006) Midlatitude westerlies, atmospheric CO2, and climate change during the ice ages. *Paleoceanography* 21.
44. Kohfeld KE, et al. (2013) Southern Hemisphere westerly wind changes during the Last Glacial Maximum: Paleo-data synthesis. *Quat Sci Rev* 68:76–95.
45. Sime LC, et al. (2013) Southern Hemisphere westerly wind changes during the last glacial maximum: Model–data comparison. *Quat Sci Rev* 64:104–120.
46. Hallberg R, Gnanadesikan A (2006) The role of eddies in determining the structure and response of the wind-driven southern hemisphere overturning: Results from the Modeling Eddies in the Southern Ocean (MESO) project. *J Phys Oceanogr* 36:2232–2252.
47. Abernathey R, Marshall J, Ferreira D (2011) The dependence of Southern Ocean meridional overturning on wind stress. *J Phys Oceanogr* 41:2261–2278.
48. Munday DR, Johnson HL, Marshall DP (2012) Eddy saturation of equilibrated circumpolar currents. *J Phys Oceanogr* 43(3):507–532.
49. Adkins JF, McIntyre K, Schrag DP (2002) The salinity, temperature, and delta18O of the glacial deep ocean. *Science* 298(5599):1769–1773.
50. Broecker WS, Takahashi T (1978) The relationship between lysocline depth and the in situ carbonate in concentration. *Deep-Sea Res* 25:65–95.
51. Skinner L (2009) Glacial - interglacial atmospheric CO_2 change: A possible standing volume effect on deep-ocean carbon sequestration. *Climates of the Past* 5:537–550.